Thermodynamic Assessment of the Chemical Durability of Refractory Lining in Anode Baking Furnaces

Trond Brandvik[1], Arne Petter Ratvik[2] and Tor Grande[3]
1. PhD Candidate
3. Professor
Department of Materials Science and Engineering, Norwegian University of Science and Technology (NTNU), Trondheim, Norway
2. Senior Research Scientist, SINTEF Materials and Chemistry, Trondheim, Norway
Corresponding author: trond.brandvik@ntnu.no

Abstract

The aluminosilicate refractory lining in anode baking furnaces undergoes thermal cycling and are exposed to harsh chemical environments. Consequently, the thermal stability and chemical durability of the refractory material is important for the lifetime of the lining. Here, we present a thermodynamic assessment of the stability of the aluminosilicate materials resembling the chemical environment of the anode baking furnace. Volatile species (NaF, $NaAlF_4$, SiO, CO, etc.) from anodes were identified based on typical chemical composition of green anodes. The most likely chemical reactions of the volatile species and the oxide components in the lining are evaluated. The variation in the volatility of substances due to the thermal cycling and reducing conditions during anode baking was examined in particular. Changes in the mineralogical composition in the lining were predicted based on the thermodynamic calculations and these are summarized in form of isothermal predominance phase diagrams. Formation of sodium aluminosilicate phases and volatile SiF_4 are proposed to be the main consequence of the chemical degradation of the lining due to traces of the cryolite in the green anodes.

Keywords: Anode baking furnace; refractory lining; degradation.

1. Introduction

Carbon anodes constitute an important part in the process of aluminum electrolysis [1,2]. Today, mostly pre-baked carbon anodes are used in modern electrolysis plants due to their higher current efficiency, lower cell voltage and lower energy consumption, compared to the Søderberg anodes [3,4]. The production of pre-baked anodes takes place in anode baking furnaces, separated from the electrolysis process. The principle of pre-baked anode production is quite similar from plant to plant, with some variations with respect to the furnace design [5], i.e. open or closed furnace. Green anodes, made out of coke, recycled anode butts and pitch, are stacked within the furnace and exposed to thermal treatment. As the green anodes are heated up, the structural integrity is reduced when reaching the softening point of the pitch [5]. To prevent any deformation, the green anodes are placed in a confined space (the pit) with no room for movement. To avoid carbon oxidation during baking, the anodes are covered with packing material, usually fine-grained carbon materials such as petroleum coke or metallurgical coke [5]. The recycled anodes used as a precursor in green anode production originates from the electrolysis cell, where the anodes are taken out of operation when they reach approximately 20-25 % of their original size. Besides the anode cover materials, the anodes are exposed to the cryolite bath during operation, and some of the bath and anode cover materials are transferred with the anodes. Impurities, like sodium and fluorine, originating from frozen bath and anode cover materials, are therefore found in increased amounts in the green anodes compared to the expected amounts based on the impurity level of the petroleum coke [1,6].

In the anode baking furnace, the anodes are separated from the hot flue gas by aluminosilicate refractory walls. The operational temperature in the furnace cycles from ambient conditions to 1200-1300 °C in cycles of 20-30 days. During the heat cycle, the cryolite contamination in the green anodes will evaporate as gas species such as NaF and $NaAlF_4$. The presence of such gaseous species will, together with the temperature cycling under reducing conditions, create harsh operational environments for the refractory walls. In time, the refractory wall will degrade causing its operational performance to decrease, and ultimately lead to the need of replacement of the lining [7,8].

Mineralogical changes in refractory materials due to exposure to sodium and fluorine containing compounds have been thoroughly investigated during the last couple of decades [1,2,7–18]. The focus has primarily been on cathode refractory lining in aluminum electrolysis cells. When aluminosilicate refractories are exposed to sodium fluoride, a series of reactions occur, depending on the silica/alumina ratio in the bricks and the amount of fluoride. The main reaction products are the sodium aluminosilicate phases nepheline ($NaAlSiO_4$) and albite ($NaAlSi_3O_8$), together with cryolite (Na_3AlF_6) and β-alumina ($NaAl_9O_{14}$ or $NaAl_{11}O_{17}$) [9,10]. In addition, both SiF_4 and $NaAlF_4$ have been detected during melt intrusion, constituting the dominating gas specie for high and low silica content respectively [11]. The phase stability of aluminosilicate refractories during NaF exposure has been summarized in a degradation map, primarily based on mass balances [9]. Later, Tschöpe et al. [17] investigated the phase stability in aluminosilicate refractories during exposure to Na(g). The result was summarized in a similar degradation map. Autopsy of a lining from anode baking furnaces have revealed the presence of mullite ($Al_6Si_2O_{13}$), corundum and cristobalite, in addition to an amorphous phase [1,2,7]. The amorphous phase was most abundant close to the anode side of the refractory, corresponding with elevated sodium content in the samples. No sign of fluorides was found in the spent lining [1,2,7].

In this work, a thermodynamic assessment of the chemical stability of the aluminosilicate refractories during anode baking is reported. First, possible reactions between the refractory material and volatile fluorides originating from the recycled anode butts are evaluated. These findings are summarized in form of degradation maps, and compared to similar findings for the degradation of refractory materials in aluminum electrolysis cells. Finally, the effect of other trace impurities in the green anodes and the effect of reducing conditions during the baking process are evaluated.

3. Method

In order to investigate phase stability in aluminosilicate refractories during exposure of volatile sodium fluorides, a thermodynamic assessment was carried out. The thermochemical software FactSage (version 7.0) was used to carry out equilibrium calculations through minimization of Gibb's energy. FactSage is a thermochemical software containing various modules and databases, enabling the user to do a variety of equilibrium calculations [19]. In this work, the *Equilibrium* module has been used in combination with the *FactPS* database to analyze the phase composition during various amounts of NaF and $NaAlF_4$. The objective of this assessment has been to predict chemical stability for aluminosilicate materials as a function of NaF or $NaAlF_4$ exposure. The compositional range from pure silica to pure alumina was thus investigated. From a refractory corrosion perspective, a "worst case" scenario has been investigated, with increasing amount of volatile sodium fluorides at a temperature in the upper region of the operational conditions (1300 °C).

3. Results

3.1. Reaction with Volatile Fluorides

The major gas species in equilibrium with liquid cryolite at 1300 °C are $NaAlF_4$ and NaF described by the chemical equilibrium

$$Na_3AlF_6(liq) = 2\ NaF(g) + NaAlF_4(g) \quad (1)$$

The partial pressure of the volatile fluorides is in the range of 10^{-2} ($NaAlF_4$) and 10^{-1} bar (NaF) at 1300 °C. The chemical reaction of these two volatile fluorides with each of the two main components in the refractory material (SiO_2 or Al_2O_3) was investigated in order to determine the oxide stability for each combination. $NaAlF_4$ is found to be coexistent with Al_2O_3, while NaF reacts with Al_2O_3 according to Equation 2. SiO_2, on the other hand, is not coexistent with neither NaF nor $NaAlF_4$, and reacts according to Equations 3 and 4. Reaction 2 and 3 are strongly shifted to the right, while reaction 4 is far more sensitive to the partial pressure of the two gases.

$$4NaF(g) + 14Al_2O_3(s) = 3NaAl_9O_{14} + NaAlF_4(g) \quad (2)$$

$$NaAlF_4(g) + 4SiO_2(s) = SiF_4(g) + NaAlSi_3O_8 \quad (3)$$

$$4NaF(g) + 5SiO_2(s) = 2Na_2Si_2O_5 + SiF_4(g) \quad (4)$$

This simple analysis illustrates that the presence of either SiO_2 or Al_2O_3 will result in formation of sodium aluminosilicates, sodium disilicate, β-alumina and volatile $SiF_4(g)$, where the latter will be transported out of the anode baking furnace.

3.2. $NaAlF_4$ Exposure

The degradation map for aluminosilicate refractories due to reaction with $NaAlF_4$ is shown in Figure 1. The map is constructed based on a combination of the thermodynamic assessment and the mass balances of the dominating reactions found by thermodynamic calculations. This is not a true phase diagram, but rather a diagram presenting the thermodynamically stable condensed phases for a given material composition and amount of $NaAlF_4$. Six regions with the corresponding stable condensed phases for each region are displayed in the diagram. With increasing amount of $NaAlF_4$ for a given composition of aluminosilicate material, a series of chemical reactions occur. The red arrow in Figure 1 indicates the reaction path for a refractory lining with 70 mol% SiO_2 and 30 mol% Al_2O_3 when exposed to an increasing amount of $NaAlF_4$.

The main reactions in region 1, 2 and 3 along the reaction path are summarized in Table 1. In Figure 2, the concentrations of each specie during the same reaction path are given as a function of the amount of $NaAlF_4$. In between region 1, 2 and 3, there are regions with no change in phase composition except the increasing activity of $NaAlF_4$. These are the regions that only have two stable condensed phases. The constant amount of phases in these regions is explained by Figure 3, where the chemical potential for the main gaseous species, $NaAlF_4$ and SiF_4, is plotted along the reaction path. In region 1, 2 and 3 the chemical potential for $NaAlF_4$ is constant, while it increases in the intermediate regions. At some point, the chemical potential reaches the threshold for the next reaction, indicated by the boundaries in Figure 1. There are some discrepancies between the boundaries in the degradation map in Figure 1 and the region borders in Figures 2 and 3.

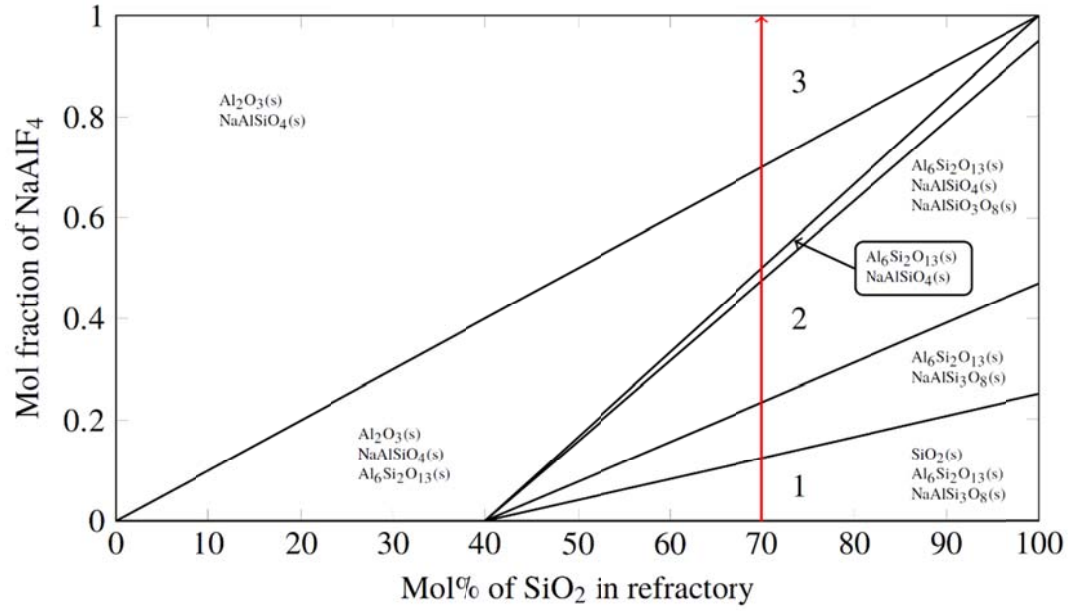

Figure 1. Phase stability for aluminosilicate refractory materials during exposure of $NaAlF_4$. The phase composition is given by the mole percentage of SiO_2 in the refractory, ranging from pure Al_2O_3 to pure SiO_2, while the exposure of $NaAlF_4$ is given as mole fraction relative to the content of aluminosilicate refractory in the system.

The degradation map is constructed based on a combination of thermodynamic calculations and mass balance considerations, while the plotted data in Figures 2 and 3 are exported directly from the equilibrium calculations. These mass balance considerations impose some simplifications to the degradation map, and consequently minor discrepancies between Figure 1 and Figures 2 and 3.

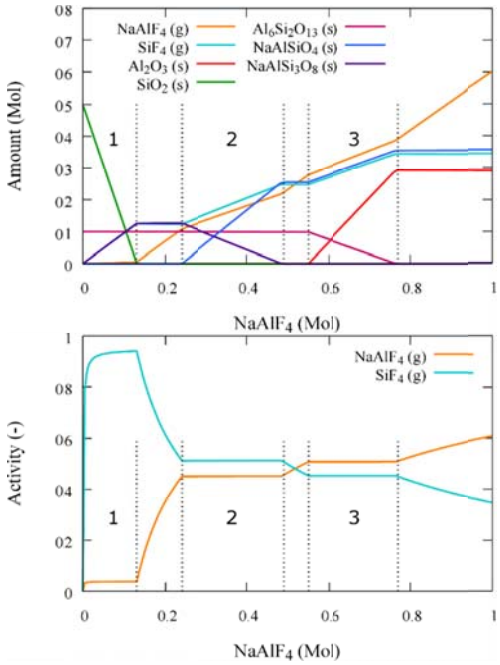

Figure 2. Phase composition of a refractory material with 70 mol% SiO_2 during $NaAlF_4$ exposure. The regions 1, 2 and 3 are related to the chemical reactions presented in Table 1.

Figure 3. Chemical activity of the main gaseous species during $NaAlF_4$ exposure to a refractory with 70 mol% SiO_2. The regions 1, 2 and 3 are related to the chemical reactions presented in Table 1.

Table 1. Chemical reactions for lining with 70 mol% SiO_2 for increasing amount of $NaAlF_4$. The region numbering is related to the indicated regions in Figure 1.

Region	Chemical reaction
1	$NaAlF_4 + 4SiO_2 = SiF_4 + NaAlSi_3O_8$
2	$NaAlSi_3O_8 + NaAlF_4 = SiF_4 + 2NaAlSiO_4$
3	$Al_6Si_2O_{13} + NaAlF_4 = SiF_4 + 3Al_2O_3 + NaAlSiO_4$

The main conclusion from the consideration of exposure of aluminosilicate refractories to $NaAlF_4$ are that phases in the pristine material (SiO_2 and $Al_6Si_2O_{13}$) are consumed in the reaction with $NaAlF_4$, while $NaAlSiO_4$ and SiF_4, with $NaAlSi_3O_8$ as an intermediate compound, are formed.

3.3. NaF Exposure

A corresponding degradation map for the aluminosilicate refractory lining under NaF exposure is constructed in the same manner, and is presented in Figure 4. The map has some similarities with the diagram reported by Schøning et al. in 1999 [9], which was constructed by considering only the mass balances of the dominating reactions proposed by the authors. The use of thermochemical software, in addition to mass balance considerations, has enabled the identification of several other stability regions resulting in a more complex diagram. This is the same approach as Tschöpe et al. [17] used to construct the degradation map for cathode lining under Na(g) exposure. The diagram can be divided in two main compositional regions, delimited by the mullite composition at 40 mol% SiO_2. The main chemical reactions occurring for increasing NaF exposure to lining with 0 to 40 mol% SiO_2 are given in Table 2. At higher silica content, the reaction paths are less straightforward, due to the complexity of the stability regions. A reaction path for lining with 70 mol% SiO_2 during increasing NaF exposure is presented in Table 3.

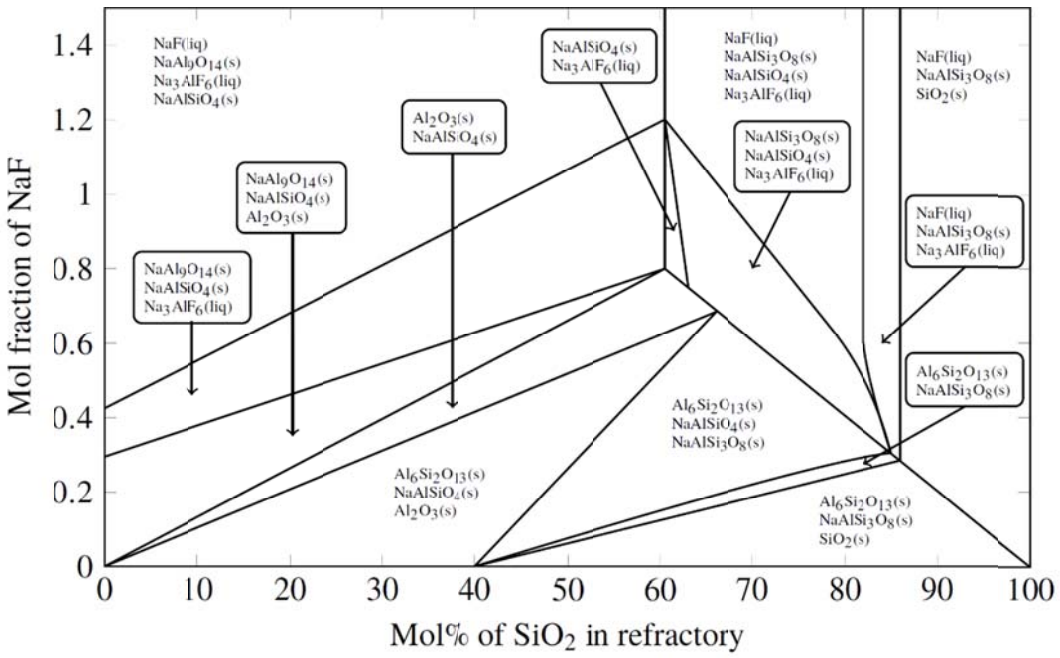

Figure 4. Phase stability for aluminosilicate refractory materials during exposure of NaF. The phase composition is given by the mole percentage of SiO_2 in the refractory, ranging from pure Al_2O_3 to pure SiO_2, while the exposure of NaF is given as mole fraction relative to the content of aluminosilicate refractory in the system.

Table 2. Main chemical reactions for increasing NaF exposure to lining with 0 to 40 mol% SiO_2.

Region	Chemical reaction
1	$3Al_6Si_2O_{13}(s) + 8NaF(g) = 5Al_2O_3(s) + 6NaAlSiO_4(s) + 2NaAlF_4(g)$
2	$4Al_2O_3(s) + 8NaF(g) + 3SiF_4(g) = 3NaAlSiO_4(s) + 5NaAlF_4(g)$
3	$14Al_2O_3(s) + 4NaF(g) = 3NaAl_9O_{14}(s) + NaAlF_4(g)$
4	$2NaF(g) + NaAlF_4(g) = Na_3AlF_6(liq)$

Table 3. Main chemical reactions for increasing NaF exposure to lining with 70 mol% SiO_2.

Region	Chemical reaction
1	$2Al_6Si_2O_{13}(s) + 35SiO_2(s) + 12NaF(g) = 12NaAlSi_3O_8(s) + 3SiF_4(g)$
2	$8Al_6Si_2O_{13}(s) + 48NaF(g) + 23SiF_4(g) = 13NaAlSi_3O_8(s) + 35NaAlF_4(g)$
3	$4Al_6Si_2O_{13}(s) + 24NaF(g) + 5SiF_4(g) = 11NaAlF_4(g) + 13NaAlSiO_4(s)$ $8NaAlSi_3O_8(s) + 8NaAlF_4(g) = 16NaAlSiO_4(s) + 8SiF_4(g)$
4	$2NaF(g) + NaAlF_4(g) = Na_3AlF_6(liq)$ $2NaAlSiO_4(s) + SiF_4(g) = NaAlSi_3O_8(s) + NaAlF_4(g)$

NaF exposure to aluminosilicate refractories causes consumption of the virgin phases (SiO_2, Al_2O_3 and $Al_6Si_2O_{13}$), while nepheline and β-alumina, or albite and nepheline are the main reaction products, in addition to SiF_4 and $NaAlF_4$, depending on the refractory composition.

3.4. Summary of Fluoride Exposure

The predominance diagrams shown in Figures 1 and 4 represent a "worst case" scenario. The partial pressure of NaF and $NaAlF_4$ at 1300 °C is in the range of 10^{-2} to 10^{-1} bar, and combined with the flow of flue gas through the furnaces, the real partial pressure of these volatile fluoride gasses is most likely considerably lower. From an industrial point of view, the interesting parts of the degradation maps are thus the regions in the diagrams with low content of fluorides. When only addressing the lower parts of the diagrams, the number of relevant phases become considerably lower, including only oxide phases. Post-mortem analysis of refractory lining with 60 mol% silica reported that only silica, alumina, mullite and an amorphous phase were present [1,2,7]. This is in accordance with the degradation maps developed in this work. The presented degradation maps should therefore be helpful for post-mortem analysis of spent refractory lining in anode baking furnaces where aluminosilicate materials are used.

3.5 Reducing Atmosphere

At elevated temperatures, volatile hydrocarbons and CO will evaporate from the green anodes leading to a reducing atmosphere in the furnace. The equilibrium partial pressure for CO (p_{CO}) is governed by the Boudouard reaction and is presented in Equation 5.

$$2CO(g) = CO_2(g) + C(s) \quad (5)$$

As the temperature varies during a heat cycle, p_{CO} changes accordingly. Equilibrium data for Equation 5 is presented in Figure 5, showing a rightwards shift in the chemical equilibrium as the temperature decreases. In the upper left part of the diagram, the gas mixture is stable and the partial pressure of CO_2 (p_{CO_2}) can be found for a given partial pressure of CO. In the lower right part of the diagram, the gas mixture is unstable, resulting in carbon deposition. A decrease in the temperature causes the deposition range to increase, as showed in Figure 5. The ratio of p_{CO} and p_{CO_2} is also governing the partial pressure of O_2 (p_{O_2}), via Equation 6.

$$CO_2(g) = CO(g) + ½O_2(g) \quad (6)$$

By fixing the temperature and p_{CO_2}, p_{O_2} can be calculated as a function of p_{CO}. Figure 6 shows how the partial pressure of oxygen varies with temperature, p_{CO_2} and p_{CO}. p_{O_2} varies with several orders of magnitude as a response to changes in temperature or the p_{CO_2}/p_{CO} ratio.

Separate calculations were carried out to investigate the influence of reducing conditions on the phase equilibria between fluorides and the aluminosilicates. These calculations demonstrate that the phase stability presented in Figures 1 and 4 is not significantly affected by the reducing atmosphere due Equation 5.

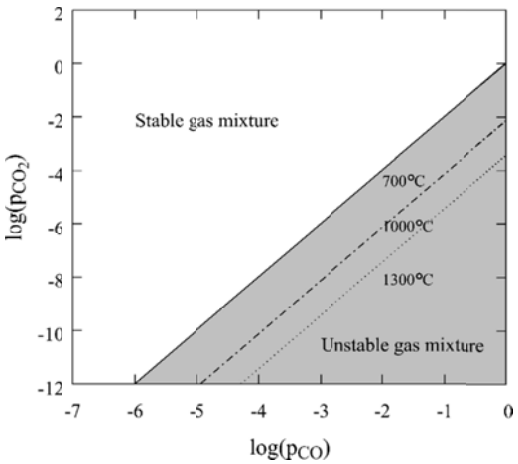

Figure 5. Equilibrium data for the Boudouard reaction (Equation 5), presented for 1300 °C, 1000 °C and 700 °C. The grey area indicates unstable gas mixture resulting in carbon deposition.

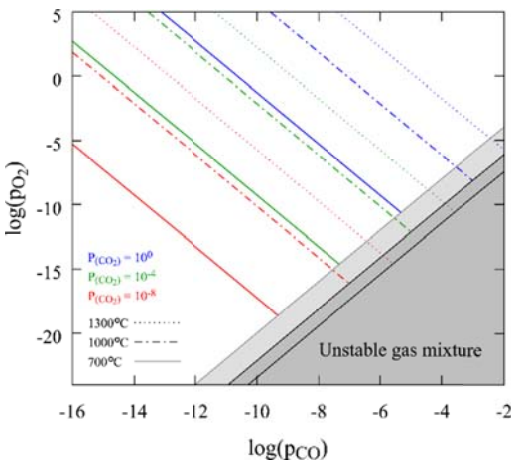

Figure 6. Equilibrium data for Equations 5 and 6 for 1300 °C, 1000 °C and 700 °C. The grey area indicates unstable gas mixture resulting in carbon deposition. The colored lines are plotted for fixed p_{CO_2}, and the line types indicate various isothermal conditions.

3.6. Carbon deposition

As the temperature varies during a heat cycle, there will be periods where the temperature is sufficiently low to cause carbon deposition. Autopsies of spent linings report blackening of the refractories close to the anode side, which is confirmed to be caused by carbon deposition [7]. The refractory wall is built up with flexible gaps allowing the wall to expand and contract with the temperature variations. The carbon deposited in these gaps reduce the wall's flexibility and will eventually cause internal stresses to build up during the heat cycle.

As shown in Figure 5, carbon deposition is also possible during anode cooling in the baking process since the region of the CO-CO_2 gas mixture becomes reducing as the temperature is going down.

4. Conclusion

Exposure of aluminosilicate refractories to gaseous sodium fluorides cause the transformation of the phases (corundum, cristobalite and mullite) in the pristine materials into β-alumina, nepheline and albite, in addition to gaseous SiF_4 and $NaAlF_4$. The phase stability of the pristine material due to NaF and $NaAlF_4$ exposure was summarized in isothermal predominance diagrams. From an industrial point of view, only the parts of the diagrams associated with low fluoride exposure is of interest, due to the expected partial pressures of gaseous sodium fluorides in the furnace. The diagrams correspond with reported data from spent refractory lining, showing that such diagrams are helpful when analyzing post-mortem samples. The presence of CO in the furnace shifts the atmosphere towards a more reducing nature. The prediction of phase stability in the isothermal predominance diagrams is however not influenced significantly by the presence of CO.

5. Acknowledgement

Financial support from the Norwegian Research Council and the partners Hydro, Alcoa, Elkem Carbon and Skamol through the project ”Reactivity of Carbon and Refractory Materials used in metal production technology” (CARMA) is acknowledged.

6. References

1. P. Prigent, M.L. Bouchetou, Gaseous corrosion of alumino-silicate refractories in anode baking furnaces used for aluminium produciton part 1, *Interceram*, 58 (2009) 121–126.
2. P. Prigent, M.L. Bouchetou, Gaseous corrosion of alumino-silicate refractories in anode baking furnaces used for aluminium produciton part 2, *Interceram*, 58 (2009) 202–209.
3. E.H.M. Moors, Technology strategies for sustainable metals production systems: a case study of primary aluminium production in The Netherlands and Norway, *J. Clean. Prod*., 14 (2006) 1121–1138.
4. H.-G. Schwarz, S. Briem, P. Zapp, Future carbon dioxide emissions in the global material flow of primary aluminium, *Energy*, 26 (2001) 775–795.
5. F.H. Becker, F. Goede, Ring pit furnaces for baking of high quality anodes - an overview, *Alum. 82*, 9 (2006).
6. A. Radjenović, Properties of carbon anode components for aluminium production, *Nafta*, 63 (2012) 111–114.
7. P. Prigent et al., The effect of the addition of fine andalusite particles in refractory bricks on gaseous corrosion, *JOM*, 60 (2008) 58–63.
8. F. Brunk, Corrosion and behavior of firecal bricks usen in the flues of open anode baking furnaces, *Light Met.*, (1995) 641–646.
9. C. Schøning, T. Grande, O.-J. Siljan, Cathode refractory materials for aluminium reduction cells, *Light Met.*, (1999) 231–238.
10. O.-J. Siljan, T. Grande, C. Schøning, Refractories for aluminium electrolysis cells part 1 - Deterioration mechanisms based on phase equilibria, *Alum. 77 Jahrgang*, (2001) 294–300.
11. O.-J. Siljan, T. Grande, C. Schøning, Refractories for aluminium electrolysis cells part 2 - Physical properties of penerating melt, reduction by metals and volatile fluorides, *Alum. 77 Jahrgang*, (2001) 385–390.
12. O.-J. Siljan, T. Grande, C. Schøning, Refractories for aluminium electrolysis cells part 3 - Laboratory test for cryolite resistance, *Alum. 77 Jahrgang*, (2001) 610–615.
13. O.-J. Siljan, T. Grande, C. Schøning, Refractories for aluminium electrolysis cells part 4 - Comparison of laboratory investigations and autopsies of pot linings, *Alum. 77 Jahrgang*, (2001) 809–814.
14. O.-J. Siljan, C. Schoning, T. Grande, State-of-the-art alumino-silicate refractories for al electrolysis cells, J. Miner. Met. Mater. Soc., 54 (2002) 46–55.
15. C. Schøning, T. Grande, The stability of refractory oxides in sodium-rich environments, *JOM*, 58 (2006) 58–61.
16. K. Tschope et al., Chemical degradation of cathode linings in hall-heroult cells - an autopsy study of three spent pot linings, *Metall. Mater. Transcations B*, 43B (2012) 290–301.
17. K. Tschöpe, J. Rutlin, T. Grande, Chemical degradation map for sodium attack in refractory linings, *Essent. Readings Light Met. Electrode Technol. Alum. Prod*., 4 (2013) 978–983.
18. J. Butter, A. Bongers, Alterations of anode baking furnace bricks during operation, *Light Met*., (1995) 633–639.
19. C.W. Bale et al., FactSage thermochemical software and databases — recent developments, *Calphad*, 33 (2009) 295–311.